POLITECNICO
MILANO 1863

Master of Science in Space Engineering

Space Propulsion
Final Project

Group: COOLING GUYS

Professor: Maggi Filippo

Authors:
Mina Baniamein - 10627453
Lorenzo Barbieri - 10702829
Riccardo Belgi - 10616718
Dan Borcea - 10678208
Pietro Communara - 10676981
Remo Stabile - 10940353
Gaia Trovatelli - 10582310

Academic Year 2022/2023

Abstract

As the space sector is growing fast in the last years, with an increasing demand for the launch of smaller and smaller satellites that requires very precise orbit insertion to prevent the risk of collision with other satellites or debris, space industries have to follow this trend with the consequent design and manufacture of small engines, capable of performing millimetric maneuvers to reach payloads' desired target. In the framework of designing a small liquid bi-propellant rocket system, the present work of *COOLING GUYS* Company addresses the analysis and design of an engine produced via additive manufacturing technology.

At first, it is presented the design of all the components of a kick stage working with Hydrazine and Nitrogen Tetroxide as propellant couple. After this, a discussion on different low toxic fuels is reported to present possible alternative "green" solution to Hydrazine, that is an extremely toxic fuel, dangerous for the environment and for human beings. In the same chapter is shown the design of the engine based on a specific green propellant couple, decided after a trade-off comparison. In the last section of the report, it is made an overview of the research on the possible materials and manufacture processes that can be used to produce both engines mentioned above, focusing particularly on additive manufacturing techniques and alloys compatible with them. In conclusion, together with a final comment on the results obtained for the standard conditions and two other scaled engines, one doubling the nominal thrust level and the other one halving it, there are reported some considerations on various aspects that can be investigated more in detail in a possible future work.

Nomenclature

T = Thrust $[N]$

I_s = Specific Impulse $[s]$

P_c = Combustion Chamber Pressure $[Pa]$

P_e = Exit Pressure $[Pa]$

u_e = Exit Velocity $[m/S]$

ρ = Density $[kg/m^3]$

A_e = Exit Area $[m^2]$

A_t = Throat Area $[m^2]$

A_{cc} = Combustion Chamber Cross Section $[m^2]$

ϵ = Expansion Ratio $[-]$

ϵ_c = Combustion Chamber Contraction Area Ratio $[-]$

μ = Viscosity $[Pas]$

Re_D = Reynold's Number with Pipe Diameter As Characteristic Length $[-]$

Pr_D = Prandt's Number with Pipe Diameter As Characteristic Length $[-]$

Nu_D = Nusselt's Number with Pipe Diameter As Characteristic Length $[-]$

C_R = Recovery Coefficient $[-]$

C_d = Discharge Coefficient

h_g = Convective Heat Transfer Coefficient Of The Gas $[W/m^2K]$

k_w = Conductive Heat Transfer Coefficient Of The Wall $[W/mK]$

T_0 = Total Temperature $[K]$

T_w = Wall Temperature $[K]$

T_a = Adiabatic Temperature $[K]$

$\dot{m}_p$ = Propellant Mass-Flow Rate $[Kg/s]$

$\dot{m}_{Ox}$ = Oxidizer Mass-Flow Rate $[Kg/s]$

$\dot{m}_{Fu}$ = Fuel Mass-Flow Rate $[Kg/s]$

O/F = Oxidizer To Fuel Ratio $[-]$

V_{Ox} = Oxidizer Tank Volume $[m^3]$

V_{Fu} = Fuel Tank Volume $[m^3]$

P_{Ox} = Oxidizer Tank Pressure $[Pa]$

P_{Fu} = Fuel Tank Pressure $[Pa]$

ΔP_{inj} = Pressure Losses Across Injection Plate $[Pa]$

ΔP_{feed} = Pressure Losses Across Feeding System $[Pa]$

ΔP_{cool} = Pressure Losses Across Cooling System $[Pa]$

ΔP_{valve} = Pressure Losses Across Valves $[Pa]$

ΔP_{dyn} = Dynamic Pressure Losses $[Pa]$

γ = Specific Heat Ratio $[-]$

V_{cc} = Combustion Chamber Volume $[m^3]$

A_{cc} = Combustion Chamber Lateral Surface $[m^2]$

L^* = Combustion Chamber Characteristic Length $[m]$

C_T = Thrust Coefficient $[-]$

C^* = Characteristic Velocity $[m/s]$

R = Universal Gas Constant $[J/KmolK]$

t_b = Burn Time $[s]$

t_{res} = Residence Time In Combustion Chamber $[s]$

L_{conv} = Length Of The Convergent Part Of The Nozzle $[m]$

L_{div} = Length Of Divergent Part Of The Nozzle $[m]$

θ_i = Initial Rao Angle $[deg]$

θ_e = Exit Rao Angle $[deg]$

Contents

List of Figures

List of Tables

Introduction

COOLING GUYS propulsion team was asked to design and develop a liquid propellant kick stage rocket engine for a generic orbit transfer of a small satellite. After an initial design phase of a standard bi-propellant configuration with Hydrazine (N_2H_4) and Nitrogen Tetroxide (NTO), the attention of the group shifts to a preliminary research of an alternative solution based on green fuel and HTP as oxidiser. Since 98% hydrogen peroxide is a driver of the system design, only the choice of the fuel is presented hereafter in the report, and it is based on thermochemical and physical properties of different species, their hazardousness, storability and compatibility with materials used for the engine. Decided the green propellant couple, that is RP-1/HTP, then is performed a second design of a kick-stage with this low toxic configuration, keeping the same thrust level and combustion chamber pressure, and the results obtained are compared with those of standard option.

Some constraints were given, like the inert mass budget and the total ΔV budget, that are respectively of 250 kg and 2500 m/s. From these values, and considering also the maximum loads that a small satellite can tolerate, a nominal thrust level of 400 N and combustion chamber pressure of 10 bar are selected. These results are chosen after a linear regression of data collected from a brief research on other missions with similar mass budget and an average thrust of about 400 N. All the engines considered are thought as kick-stages like in this case of study.

-Mars Express was launched on June 2, 2003 by ESA in order to explore the planet Mars and it was the first planetary mission attempted by the agency. On December 25 went into a highly elliptical initial capture orbit firing its main engine which consists of a 400 N bi-propellant liquid engine. Pressurized helium is used to force fuel into the engine (1).

-MESSENGER, launched on August 3, 2004 by NASA. The Mercury orbital insertion took place on March 18, 2011. Main propulsion was provided by the 645 N, 317 sec. I_s bi-propellant (Hydrazine and Nitrogen Tetroxide) large velocity assist (LVA) thruster. The spacecraft was designed with an additional tank intended for the storage of Helium as pressurizer (2).

-Mars Orbiter Mission, launched on November 5, 2013 by ISRO, was equipped with a motor of 440 N that performed 4 maneuvers (3).

-Electron first launch took place in 2017, his kick-stage is composed by a rocket engine that produces 120 N of thrust, and has a specific impulse around 320 seconds.

Even other components of the system are imposed by the supervisor: the type of the valves, not with throttling capability but just on/off valves; the selection of a propellant that is not self-pressurized, and the consequent sizing of an additional tank intended for pressurizing gas; the architecture of the overall system, that is pressure-fed; and the selection of a material compatible with liquids involved and with operating temperature of heat gas resulted from combustion process.

Another topic analyzed, regarding the selection of the material, is the behaviour of particular alloys during additive manufacturing processes, and the limits of these technologies used for manufacture compact rocket engines like the one in this case of study. Especially, the possibility of different alloys to be used to produce in a single block complex parts of the engine like the injection plate, combustion chamber and part of the nozzle, called printability.

In the end, an evaluation of engine up-scaling and down-scaling, respectively doubling and halving the thrust level with respect to the nominal one, was performed, pointing out benefits and drawbacks of developing engines with different scale than the initial one for this mission.

Chapter 1

Hydrazine/NTO Engine

1.1 Introduction and starting assumptions

For the nominal toxic-fuel design the following values were the input for the design phase. The O/F ratio is chosen via NASA's CEA code in order to maximize the specific impulse of the propulsion unit as shown in the table below.
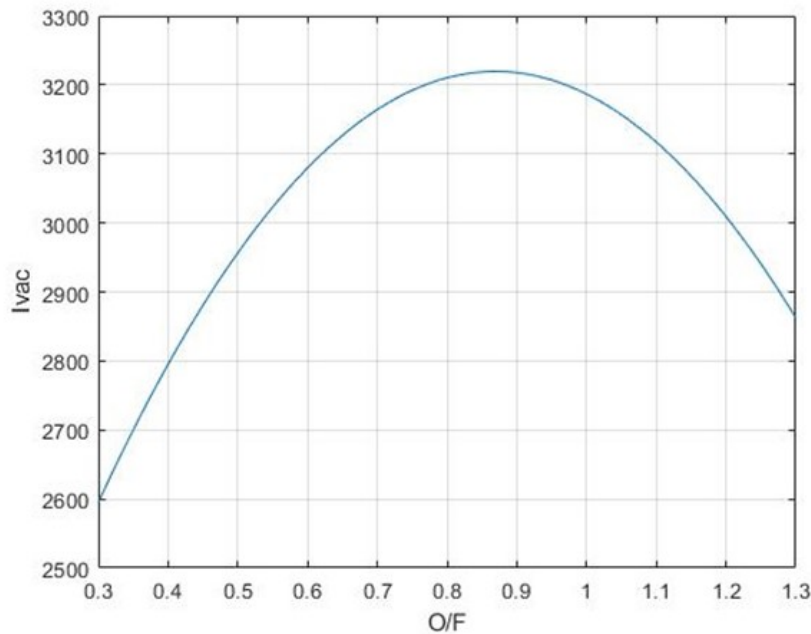
Figure 1.1: I_{vac} to O/F correlation

Still from CEA software, by using the chosen oxidizer-fuel ratio, is possible to retrieve other properties, such as the combustion chamber temperature, the molecular mass and the specific heat ratio of the combustion products at the beginning of the chamber. For the study of the performance and for running the CEA software the isoentropic frozen model is used.

Δv $[\frac{m}{s}]$	m_{inert} [kg]	P_c [bar]	T [N]	ϵ [-]	γ [-]	M_{mol} $[\frac{Kg}{kmol}]$	O/F [-]	C_p $[\frac{KJ}{KgK}]$
2500	250	10	400	200	1.26	18	0.86	2.389

Table 1.1: Performance Analysis Inputs

Data such as the molar mass or the constant pressure specific heat coefficient is obtained from the CEA code. Since an analysis of the engine up-scaling and down-scaling is requested, the same computations were performed three times in the following conditions: Selected thrust, doubled and halved thrust. The outputs of the general performance analysis are the following:

Quantity	Units	Nominal Thrust	Halved Thrust	Doubled Thrust
m_p	$[kg]$	321.43	321.43	321.43
m_{Ox}	$[kg]$	148.66	148.66	148.66
m_{Fu}	$[kg]$	172.87	172.87	172.87
$\dot{m}_p$	$[\frac{kg}{s}]$	0.1275	0.0638	0.2551
$\dot{m}_{Ox}$	$[\frac{kg}{s}]$	0.0590	0.0295	0.1179
$\dot{m}_{Fu}$	$[\frac{kg}{s}]$	0.0686	0.0343	0.1371
c_f	$[-]$	1.9090	1.9090	1.9090
I_{sp}	$[s]$	319.7107	319.71	319.71
I_{tot}	$[N*s]$	1.0085e+06	1.0085e+06	1.0085e+06
t_{burn}	$[s]$	2521	5042	1260
A_{cc}	$[m^2]$	$8.3815*10^{-4}$	$4.2810*10^{-4}$	0.0017
A_t	$[m^2]$	2.0954e-04	1.0477e-04	4.1907e-04
A_e	$[m^2]$	0.0419	0.0210	0.0838
u_e	$[m/s]$	3070.2	3070.2	3070.2

Table 1.2: Outputs of the P.A.

The results listed above are used as inputs for the designing and sizing phase of all the components. It should be noticed that values such as the exit velocity u_e are the same among all levels of T as it is dependant exclusively on the pressure ratio between throat and exit. As the geometry of the nozzle is simply scaled up or down these values do not change across the engine lineup.
As I_{sp} is an intensive quantity, it does not vary across the engine lineup.
Once the expansion and pressure ratios are fixed, the only quantities that can have an impact on the T level are, respectively, the throat area and the mass flow rate.
Doubling the mass flow rate to double the thrust level reduces in half the burning time, as they are directly proportional quantities.
Further considerations regarding the challenges of up and down scaling the engine will follow.

1.2 Preliminary design and performances evaluation of Hydrazine/NTO Engine

1.2.1 Nozzle

When designing the nozzle, both a conical and bell-shaped nozzle where considered.
Using the GPA Outputs as inputs for this phase and following the procedure described in Appendix A.1, the following results are obtained:

Parameter	Unit	Normal Thrust	Halved Thrust	Doubled Thrust
C_f	[-]	1.9090	1.8687	1.8687
A_t	$[m^2]$	2.0954e-04	1.0477e-04	4.1907e-04
A_e	$[m^2]$	0.0419	0.0210	0.0838
α	$[deg]$	15	15	15
β	$[deg]$	40	40	40
L_{conv}	$[m]$	0.0139	0.0099	0.0197
L_{div}	$[m]$	0.2403	0.1699	0.3399
θ_i	$[deg]$	37.91	37.91	37.91
θ_e	$[deg]$	12.65	12.65	12.65
$L_{RAO-div}$	$[m]$	0.1442	0.1020	0.2039
λ	[-]	0.9830	0.9830	0.9830
η	[-]	0.970	0.970	0.970

Table 1.3: Nozzle Design Outputs

It is possible to notice that all the properties that depend exclusively on the geometry of the nozzle (in terms of angles), such as the λ and η coefficients, remain the same for all the different levels of T. What changes are exclusively the areas of the different sections, such as throat area and exit area, hence a larger level of thrust requires larger sections.

As mentioned in appendix A.1, a 60 % length value was chosen for the RAO approximation to reduce the size, because longer nozzles are heavier, assuming constant properties such as thickness, and especially more difficult to cool down using the regenerative cooling. Below the shape of the nominal nozzle is represented.
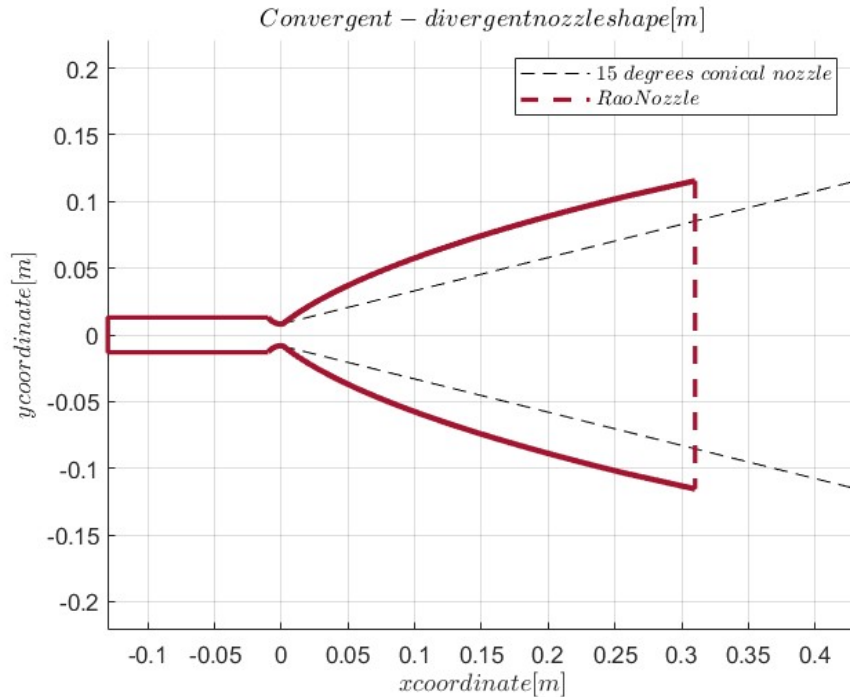

Figure 1.2: Shape of the engine using RAO model and respective reference conical nozzle

1.2.2 Injection plate

Quantity	Unit	Nominal Thrust		Halved Thrust		Doubled Thrust	
		FU	*OX*	*FU*	*OX*	*FU*	*OX*
A_{inj}	$[m^2]$	7.3442e-7	5.2765e-7	7.3444e-7	5.2765e-7	7.344e-7	5.27e-7
D_{inj}	$[m]$	9.6736e-4	8.1943e-4	9.676e-4	8.1963e-4	9.6734e-4	8.19e-4
$\dot{m}_{inj}$	$[\frac{kg}{s}]$	0.0171	0.0147	0.0171	0.0147	0.0171	0.0147
N	[-]	4	4	2	2	8	8
v_{inj}	$[\frac{m}{s}]$	23.22	19.4	23.22	19.4	23.22	19.4
ρ	$[\frac{kg}{m^3}]$	1005	1440	1005	1440	1500	1440
ΔP_{inj}	$[Pa]$	350000	350000	350000	350000	350000	350000
Holes distance	$[m]$						

Table 1.4: Like on Like Doublet Injection Values

As it can be seen the exit velocity remains constant when changing the configuration, hence it is only depending on the pressure drop in correspondence of the injection plate. The distance of the impingement point and surface and the distance between the two points are set to respectively 5.4 mm and 4 mm. The two impinging angles are set to 14.8365 (fuel) and 25.7748 (oxidizer) degrees, in order to achieve an angle of the resultant stream of 2 degrees with respect to the axial directions towards the centre, for better mixing performance. The procedure is explained in the appendix A.3. As the thrust grows more injection holes are required, and the manufacturing becomes more complex. On the other hand a much better mixing in the combustion chamber can be achieved, thus increasing the performances. The selection of the hole depends on the chosen discharge coefficient and diameter to achieve the desired exit stream velocity around 20 m/s, so the short tube with rounded entrance is the one which implies a relatively high discharge coefficient C_d of 0.88.

1.2.3 Combustion chamber

Quantity	Units	Nominal Thrust	Halved Thrust	Doubled Thrust
$L*$	$[m]$	0.899	0.899	0.899
L_c	$[m]$	0.1317	0.1365	0.1248
A_c	$[m^2]$	0.0013	6.2861e-4	0.0025
D_c	$[m]$	0.0397	0.0281	0.0562
V_c	$[m^3]$	1.8626e-04	9.3139e-5	3.7256e-4
M	[-]	0.0985	0.0985	0.0985
ϵ	[-]	6	6	6

Table 1.5: Combustion Chamber Values

The combustion chamber characteristic length L^* does not depend on the thrust level but only on the propellant couple so it is the same value across all engines. The contraction ratio instead can be fixed as a design choice. In orther to limit the heat transfer between chamber and coolant propellant the contraction ratio is selected as 6, meaning a shorter combustion chamber. It is possible now to compute the volume of the CC through the approximated relations. As the contraction ratio is fixed it is now necessary to verify a posteriori that the Mach number is compliant with the original hypothesis of 0.1 and the length can then finally computed. The impact of the Thrust level is on the size of the chamber since L^* is fixed, and is directly proportional to the mass flow rate.

1.2.4   Feeding lines

Quantity	Unit	Nominal Thrust		Halved Thrust		Doubled Thrust	
		FU	OX	FU	OX	FU	OX
v	$[\frac{m}{s}]$	9.00	9.00	9.00	9.00	9.00	9.00
D	$[m]$	0.0031	0.0024	0.0022	0.0017	0.0044	0.0034
μ	$[Pas]$	9.00e-04	9.00e-04	9.00e-04	9.00e-04	9.00e-04	9.00e-04
Re	[-]	3.1223e+04	4.4738e+04	2.2078e-04	3.1634e-04	4.4156e+04	6.3269e+04
ϵ	$[m]$	8.0469e-04	0.0010	0.0011	0.0015	5.69e-04	7.3445e-04
L	$[m]$	0.1506	0.0842	0.0974	0.0545	0.2321	0.1298
$Darcy$	[-]	0.0253	0.0245	0.0277	0.0268	0.0233	0.0225
ΔP_{inj}	$[Pa]$	350000	-	350000	-	350000	-
ΔP_{dyn}	$[Pa]$	4.0702e+04	58320	4.0702e+04	58320	4.0702e+04	58320
ΔP_{pipe}	$[Pa]$	50000	-	50000	-	50000	-
ΔP_{valve}	$[Pa]$	20684	-	20684	-	20684	-

Table 1.6: Feeding Lines Values

The velocity of the flow is imposed across all the different engines with the different thrust levels, and so were all the estimated losses along the lines.
A more powerful engine requires longer pipes and feeding lines as the mass flow rate of both fuel and oxidizer is higher.

1.2.5   Tank sizing

Quantity	Unit	Nominal Thrust			Halved Thrust			Doubled Thrust		
		FU	OX	$PRESS$	FU	OX	$PRESS$	FU	OX	$PRESS$
$P_{i,tank}$	$[Pa]$	1.59e+6	1.61e+6	1.62e+7	1.61e+6	1.61e+7	1.62e+7	1.61e+6	1.62e+6	1.62e+7
r_{tank}	$[m]$	0.3561	0.3004	0.2898	0.3561	0.3015	0.2898	0.3561	0.3004	0.2898
t_{tank}	$[m]$	0.0014	0.0012	0.0085	0.0014	0.0012	0.0085	0.0014	0.0012	0.0085
A_{tank}	$[m^2]$	1.5939	1.1341	1.0553	1.6057	1.5939	1.0553	1.5939	1.1341	1.0553
V_{tank}	$[m^3]$	0.1892	0.1136	0.1019	0.1892	0.1148	0.1019	0.1892	0.1136	0.1019
m	$[kg]$	172.86	148.66	2.6681	174.79	172.86	2.6681	172.86	148.66	2.6681
m_{tank}	$[kg]$	6.1435	3.7281	26.0359	6.2012	3.7627	26.0358	6.2013	3.76	26.032

Table 1.7: Tanks Values

All the tanks have the same characteristics as all the engines have the same specific impulse, thus the same mass of both fuel and oxidizer.Liquid propellant's tanks were design using Al2219 in order to reduce the weight of the system.Pressurant's tanks were designed using A286 as the thickness would've been to large using a regular Al-based alloy. The initial temperature of fuel and oxidizer it's chosen in order to be upon the freezing point.

1.2.6   Cooling system

As discussed in appendix A.6 several cooling strategies were investigated, with each one producing a different result in terms of both effectiveness and efficiency.
As it is the easiest case to investigate thermodynamically, the radiative cooling was the first approach to be implemented, which requires a series of 3 resistances in series. They are respectively the convective resistance, the conductive one and the radiative one, moving from the hot gas mixture towards the outside.
In order to model the convective resistance, the Nusselt number shall be computed with a suitable correlation: the needed Reynold and Prandtl numbers are calculated using the values of viscosity, density and specific heat, functions of temperature and pressure given by the CEA software. It is now possible to compute the outer temperature of the nozzle wall via nodal approach.
When at this step an engineering choice has to be performed and the thickness of the wall is fixed and has a value of 2mm.

Assuming an emissivity coefficient of 0.9 and a view factor of 1, the heat flux per unit time emitted via radiation is not enough to set the nozzle in thermal equilibrium. This leads to rising temperatures into the nozzle wall. Radiative cooling therefore is not a viable option.
Regenerative cooling was then considered.
A critical point when performing such analysis is the choice of the thickness of the nozzle wall. A good compromise between temperature on the outer surface and weight should be considered.
The total thermal power that has to be exchanged by the combustion chamber is obtained multiplying the heat flux per unit time of the chamber for its lateral surface.

$$\dot{Q}_{cc} = \dot{q_{cc}} A_{cc} \tag{1.1}$$

As a thermal equilibrium among the nozzle wall and the coolant fluid is imposed for the next step, it is possible, once the C_p and the mass flow rate of the fuel are known, to compute the ΔT in the cooling channels.

It shall be noticed that, since the thermal power is directly proportional to both the lateral surface of the combustion chamber and the fuel mass flow rate, the critical aspect of this phase is cooling the engine with halved T.

As the ΔT using fuel only would be barely enough to cool the nozzle, in order to maintain a certain margin of safety in our design, we opted for a solution in which the fuel was used to cool both combustion chamber and nozzle throat, while the oxidizer was used to cool the nozzle.

This granted a certain margin of safety in terms of the temperature reached in the channels and makes sure neither the fuel nor the oxidizer reach their boiling point.

Quantity	Unit	Nominal Thrust			Halved Thrust			Doubled Thrust		
		C.C.	Throat	Exit	C.C.	Throat	Exit	C.C.	Throat	Exit
M	[-]	0.1	1	6.07	0.1	1	6.07	0.1	1	6.07
P	[Pa]	9.94e5	5.49e5	200	9.94e5	5.49e5	200	9.94e5	5.49e5	200
T	[K]	2.54e3	2.25e3	438	2.54e3	2.25e3	438	2.54e3	2.25e3	438
a	$[\frac{m}{s}]$	1.21e3	1.14e3	505	1.21e3	1.14e3	505	1.21e3	1.14e3	505
v	$[\frac{m}{s}]$	121.62	1.14e3	3.06e3	121.62	1.14e3	3.06e3	121.62	1.14e3	3.06e3
γ	[-]	1.2397	1.2451	1.3736	1.2397	1.2451	1.3736	1.2397	1.2451	1.3736
c_{pgas}	[-]	2.38e3	2.35e3	1.70e3	2.38e3	2.35e3	1.70e3	2.38e3	2.35e3	1.70e3
μ_{gas}	$[Pa*s]$	8.28e-5	7.72e-5	1.71e-5	8.28e-5	7.72e-5	2.38e3	8.28e-5	7.72e-5	1.71e-5
λ_{gas}	$[\frac{W}{mK}]$	0.3167	0.2876	0.0518	0.3167	0.2876	0.0518	0.3167	0.2876	0.0518
ρ	$[\frac{kg}{m^3}]$	0.8464	0.5297	9.87e-4	0.8464	0.5297	9.87e-4	0.8464	0.5297	9.87e-4
A	$[m^2]$	0.0013	2.09e-4	0.0419	4.93e-4	1.04e-4	2.1e-2	0.0025	2.09e-4	0.0419
D	$[m]$	0.0397	0.0163	0.2310	0.0274	0.0115	0.1633	0.0562	0.0163	0.2310
Re	[-]	4.93e4	1.28e5	4.08e4	7.15e4	9.07e4	2.88e4	6.98e4	1.28e5	4.08e4
Pr	[-]	0.625	0.6293	0.5621	0.625	0.6293	0.5621	0.625	0.6293	0.5621
Nu	[-]	145.86	314.61	114.80	143.65	238.43	87.01	192.47	314.61	114.81
h_g	$[\frac{W}{m^2K}]$	1.16e3	5.54e3	25.74	1.79e3	5.94e3	27.59	1.08e3	5.53e3	25.74
q	$[\frac{W}{m^2}]$	1.210e6	5.520e6	2.170e4	2.40e6	5.92e6	2.33e4	1.129e6	5.52e6	3.457e4
T_{aw}	[K]	2.54e3	2.49e3	2.34e3	2.84e3	2.49e3	2.34e3	2.54e3	2.49e3	2.34e3
σ_{Bartz}	[-]	1.2147	1.2168	1.1615	1.2137	1.2168	1.1615	1.215	1.217	1.161
Q	[W]	1.77e4	3.94e3	3.78e3	1.45e4	2.11e3	2.02e3	2.09e4	7.36e3	7.06e3
ΔT_{fuel}	[K]	83.67	18.57	0	136.41	19.91	0	49.29	17.33	0
ΔT_{ox}	[K]	0	0	41.76	0	0	44.76	0	0	38.96

Table 1.8: Cooling Values

The following results are the final temperature of the oxidizer and fuel, that must be below their $T_{boiling}$, which are respectively 360K and 480K.

Quantity	Units	Nominal Thrust	Halved Thrust	Doubled Thrust
$T_{initial,fuel,ox}$	$[K]$	300	300	300
$T_{final,fuel}$	$[K]$	402	456	366
$T_{final,ox}$	$[K]$	341	344	338

Table 1.9: Temperature after cooling

Down sizing the engine is critical for the cooling problem, as the convective heat transfer coefficient is inversely proportional to the diameter elevated to an exponent greater than 1 (1.8). Therefore it is more challenging to cool a smaller combustion chamber.

Chapter 2

Green Propellant Engine

2.1   Low-toxic fuel overview

It has been selected from literature a series of fuels, that are generally considered as "green" for their lower level of toxicity with respect to Hydrazine and its derivates, and it has been analyzed their compatibility with the requirements imposed by the mission supervisor. The candidates that has been considered are light hydrocarbons, kerosene and alcohols, in particular Methanol, Ethanol, Isopropanol, Ethane, Propane, Ethene, Propene, Ethyne, Propyne and Kerosene. Within those fuels Ethane, Ethene and Ethyne have a very low density that make them inadequate for volume-limited applications [Figure 2.2]. Being a small size an important constraint for a kick-stage engine, it has been therefore decided to exclude them. Besides, light hydrocarbons are not suggested for on orbit application because of their low boiling points: this characteristic precludes their use. From these assumptions the only candidates that satisfy the operational conditions are Ethanol, Isopropanol and Kerosene. These three hydrocarbons appear to be the most promising options in terms of physical properties and theoretical performance. [Figure 2.1].
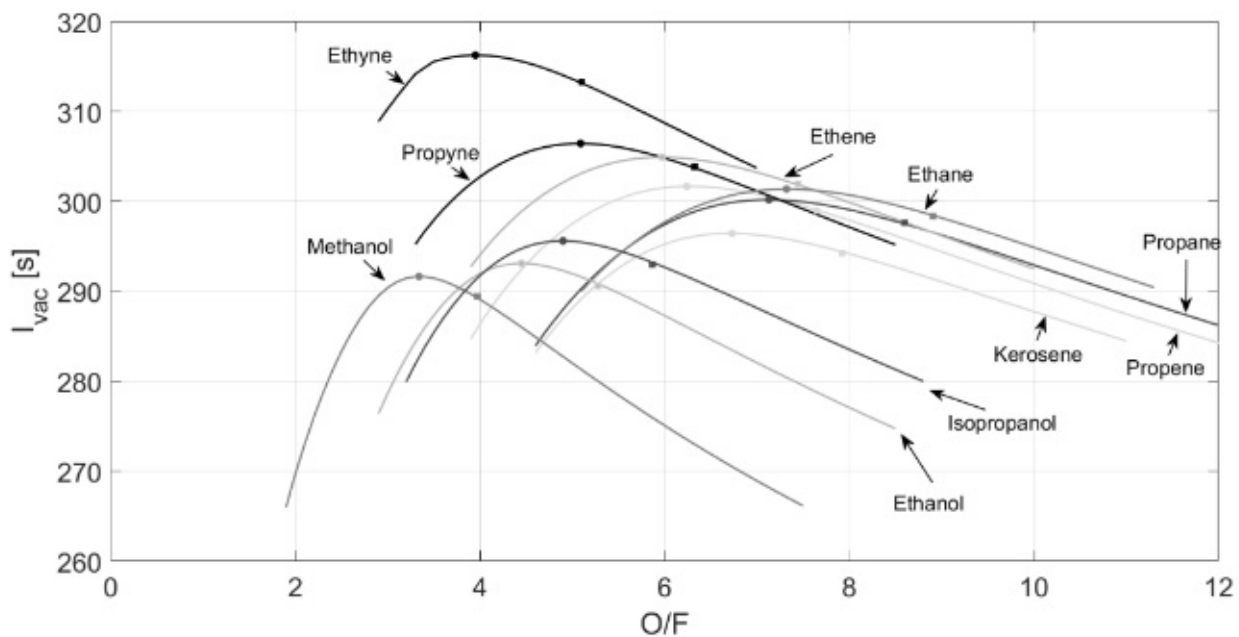

Figure 2.1: I_s comparison between low-toxic fuels with respect to O/F ratio
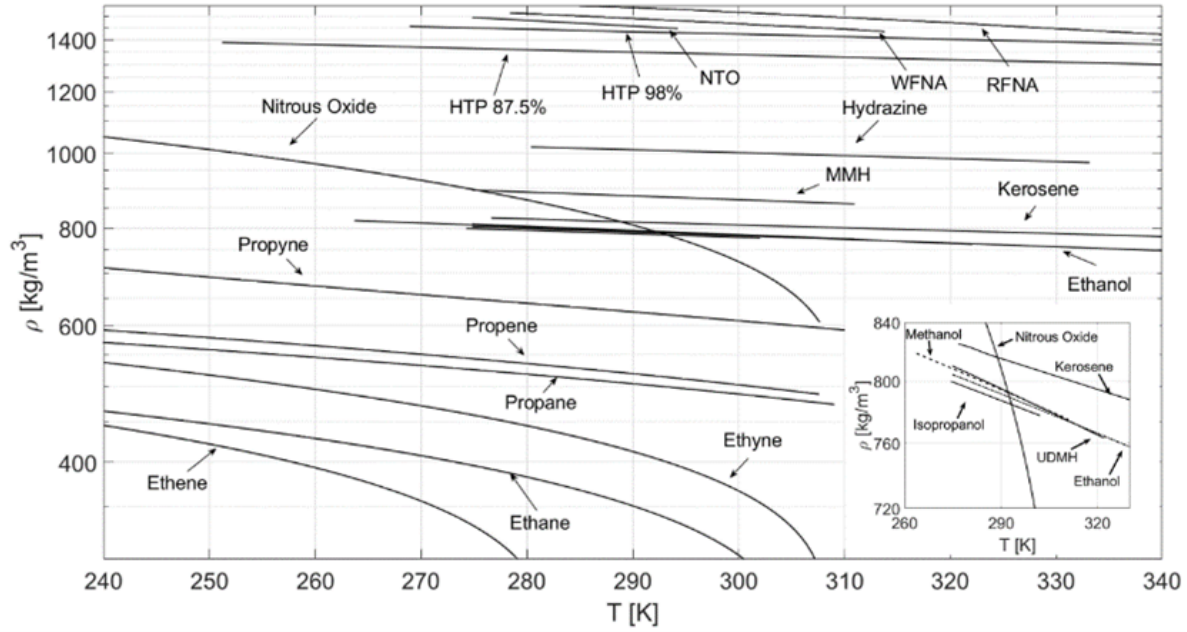
Figure 2.2: Comparison between low-toxic fuel densities with respect to temperature variation

The selection procedure between these three fuels has been conducted, first of all, by the analysis of the performance trend of 98% HTP/Hydrocarbon mixtures varying their mixture ratios. It has been observed that the performance is slightly higher for Kerosene than for Ethanol and Isopropanol.

The optimum mixture ratio has a higher value for Kerosene, which indicates how its combustion requires a higher proportion of HTP to generate the same thrust level with respect to the other two hydrocarbons considered. HTP being the most expensive compound between the propellants considered, higher values of mixture ratio are costly. However, since HTP's density is way higher than the one of the fuels, it also brings a mass saving. The density of Kerosene, slightly higher than for the other fuels, also leads to slightly smaller and lighter fuel tank [Figure 2.3].

Figure 2.3: I_s variation of Ethanol and RP-1 with respect to O/F ratio

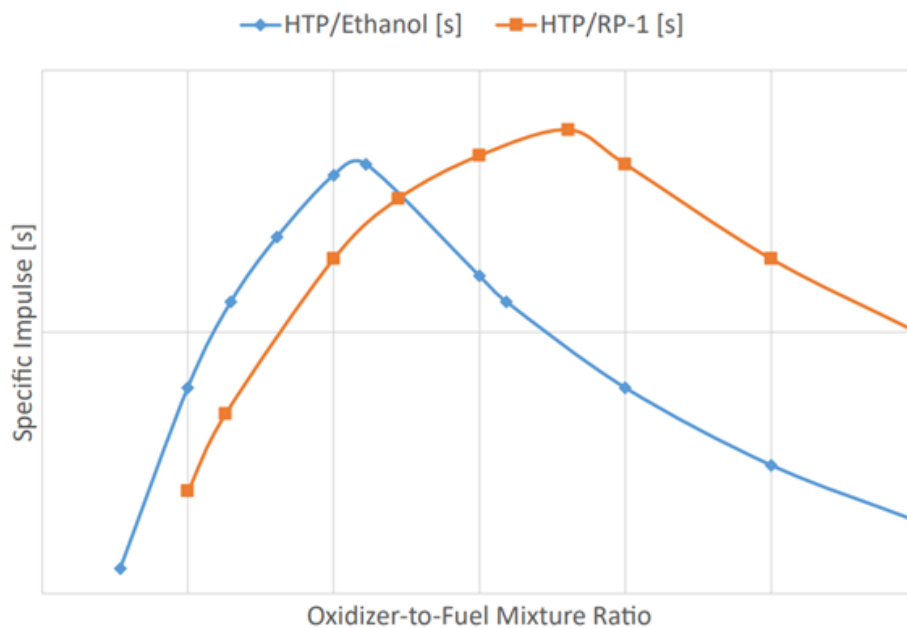From a technical perspective, tests have already been conducted with Ethanol in the framework of the FLPP Green Storable Propulsion project while no data are yet available for Kerosene to support the trade-off; Kerosene is however a well-known propellant and has already been used in combination with HTP. Based on element-level testing within the FLPP Green Storable Propulsion Project, Isopropanol is, for now, a less preferred option. Another aspect to take into account is the effect of soot production; in fact, kerosene is well known for the production of soot when operating temperatures are above 900-100°C. In on-ground conditions this could constitute an issue because a complete combustion during short firings becomes difficult to achieve; however, since in this case the engine is meant to be operating in vacuum, this effect not only would not affect the performances but would also create an insulation layer inside the nozzle, which could help for cooling it.

Given these observations, in conclusion, it has been decided to use the 98% HTP/Kerosene couple in order to maximize the specific impulse and the volume-saving. The drawback of the choice of kerosene is that, since this hydrocarbon is not hypergolic with Hydrogen Peroxide, a different design of the injection plate has become necessary.

2.2 Preliminary design and performances evaluation of Green Propellant Engine

A similar GPA is made for the green-propellant-powered engine.
The inputs of the GPA are the same as the ones used for the toxic-fuel-powered engine with the exception of the parameters regarding the fuel and oxidizer couple such as density and O/F ratio.
The O/F ratio is chosen in the same way as in for the toxic-propellant-powered engine: with the intent of maximising the I_{sp}
Data to support the choice made was collected using once again NASA CEA's code.
The I_{sp} to O/F correlation is shown in the picture below:
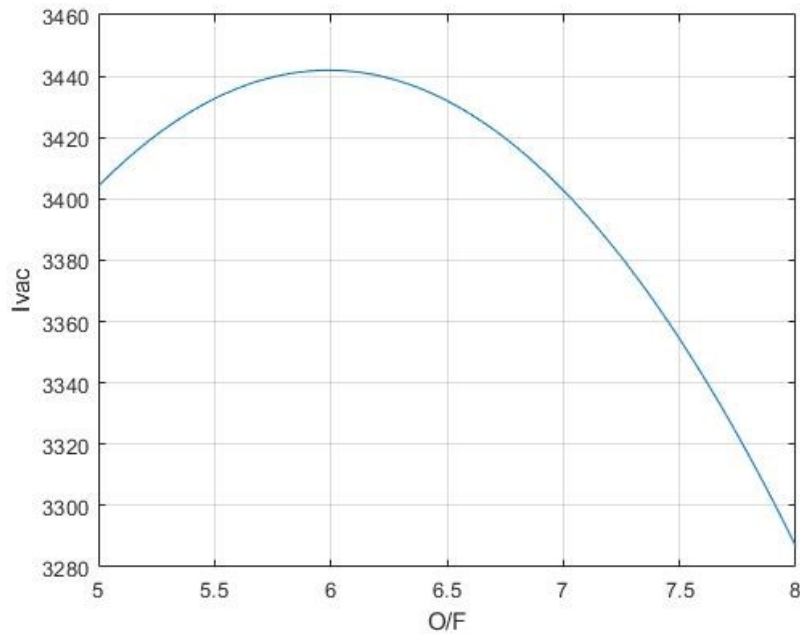

Figure 2.4: I_v to O/F correlation

The set of the input parameters used in the design phase for such engine is the following:

Table 2.1: Performance Analysis Inputs

Δv $[\frac{m}{s}]$	m_{inert} [kg]	P_c [bar]	T [N]	ϵ [-]	γ [-]	M_{mol} $[\frac{Kg}{kmol}]$	O/F [-]
2500	250	10	400	200	1.18	21.48	6

In order to have relatable quantities, the geometric properties of the engine where not changed and neither were the thrust and P_c values.
As was requested for the toxic-propellant-powered, an analysis on the up-scaling and down-scaling capability of the engine was performed.
The only changing parameters when entering this phase were the thrust and, therefore, the values of mass flow rate and throat diameter.
As I_{sp} is an intensive quantity it does not vary across the engine lineup.

Table 2.2: Outputs of the P.A.

Quantity	Units	Nominal Thrust	Halved Thrust	Doubled Thrust
m_p	[kg]	298.35	298.37	298.35
m_{Ox}	[kg]	255.75	255.76	255.75
m_{Fu}	[kg]	42.62	42.63	42.63
$\dot{m}_p$	$[\frac{kg}{s}]$	0.1211	0.0605	0.2422
$\dot{m}_{Ox}$	$[\frac{kg}{s}]$	0.1038	0.0519	0.2076
$\dot{m}_{Fu}$	$[\frac{kg}{s}]$	0.0173	0.0086	0.0346
c_f	[-]	2.0265	2.0265	2.0265
I_{sp}	[s]	336.8	336.76	336.8
I_{tot}	[N*s]	9.8575e+05	9.8575e+05	9.8575e+05
t_{burn}	[s]	2464	4928.8	1232
A_{cc}	[m²]	7.8952e-04	3.9476e-04	0.0016
A_t	[m²]	1.9738e-04	9.869e-04	3.9476e-04
A_e	[m²]	0.0395	0.0197	0.0790
u_e	[m/s]	3203.2	3203.3	3203.2

Once the expansion and pressure ratios are fixed the only quantities that can have an impact on the T level are the respectively the throat area and the mass flow rate.
Doubling the mass flow rate to double the thrust level reduces in half the burning time as they are directly proportional quantities.

2.2.1 Nozzle

The same computations as for the toxic-propellant-powered engine were performed for this section. Different values of density and propellant mass flow rate were considered, as mentioned in the inputs of the Performance analysis.The nozzle of the green-propelled-engine is characterized by the following values according to the chosen thrust level :

Table 2.3: Nozzle Design Outputs

Parameter	Unit	Normal Thrust	Halved Thrust	Doubled Thrust
c_f	[-]	2.0265	2.0265	2.0265
A_t	[m^2]	1.9738e-04	9.869e-04	3.9476e-04
A_e	[m^2]	0.0395	0.0197	0.0790
α	[deg]	40	40	40
β	[deg]	15	15	15
L_{conv}	[m]	0.0136	0.0096	0.0193
L_{div}	[m]	0.2409	0.1703	0.3406
θ_i	[deg]	37.35	37.35	37.35
θ_e	[deg]	12.13	12.13	12.13
$L_{RAO-div}$	[m]	0.1492	0.1055	0.2110
λ	[-]	0.983	0.983	0.983
η	[-]	0.975	0.975	0.975

The same considerations can be done as for the nozzle design of the toxic propellant.
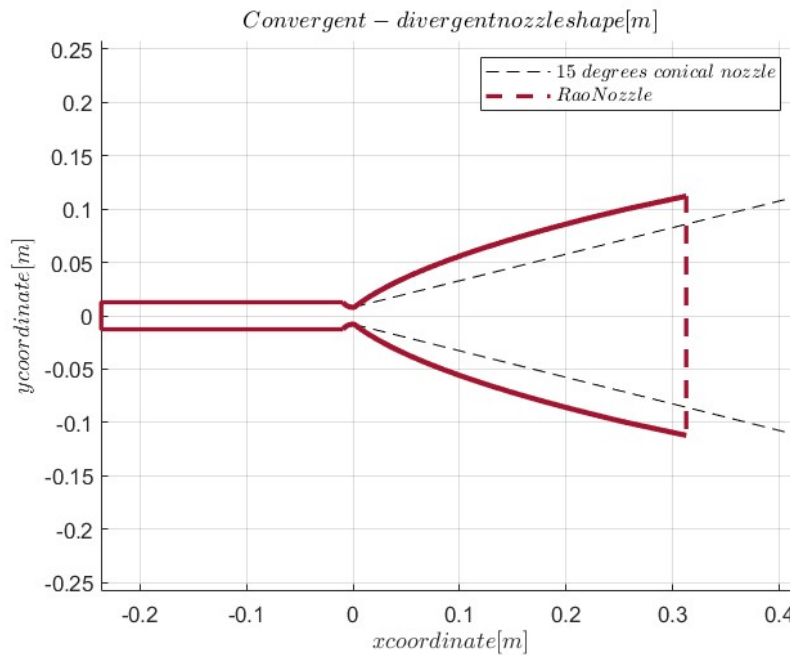

Figure 2.5: Shape of the engine using RAO model and respective reference conical nozzle

2.2.2   Injection plate

Quantity	Unit	Nominal Thrust		Halved Thrust		Doubled Thrust	
		FU	OX	FU	OX	FU	OX
A_{inj}	$[m^2]$	1.9995e-7	4.5109e-7	2.4994e-07	5.6386e-07	1.9995e-07	4.5109e-07
D_{inj}	$[m]$	5.0000e-04	7.5785e-4	5.0000e-04	8.4731e-04	5.0000e-04	7.5785e-04
$\dot{m}_{inj}$	$[\frac{kg}{s}]$	0.0035	0.0104	0.0043	0.0130	0.0035	0.0104
N	[-]	5	10	2	4	10	20
v_{inj}	$[\frac{m}{s}]$	21.4858	15.8667	21.4858	15.8667	21.4858	15.8667
ρ	$[\frac{kg}{m^3}]$	820	1450	820	1450	820	1450
ΔP_{inj}	$[Pa]$	300000	300000	300000	300000	300000	300000
Holes distance	$[m]$						

Table 2.4: Unlike Doublet Injection Values

As the propellant couple chosen is NOT hypergolic an unlike doublet injection system was chosen.
The propellant couple could turn hypergolic adding a few additives. The study of that is not goal of this paper.

2.2.3   Combustion chamber

For the given the combination of propellants (H02/RP-1), data about the characteristic length without the presence of catalyst is not retrievable from literature. To obviate this problem, an assumption has been taken comparing the performance enhancement given by the catalyst in the LO,/LH2 couple and using it as a reference to obtain a feasible value. The final chosen value is L* = 1.524m.

Quantity	Units	Nominal Thrust	Halved Thrust	Doubled Thrust
$L*$	$[m]$	1.524	1.524	1.524
L_c	$[m]$	0.2381	0.2428	0.2315
A_c	$[m^2]$	0.0012	5.9214e-4	0.0024
D_c	$[m]$	0.0387	0.0274	0.0548
V_c	$[m^3]$	3.0081e-4	1.504e-4	6.0161e-4
M	[-]	0.0994	0.0994	0.0994
ϵ	[-]	6	6	6

Table 2.5: Combustion Chamber Values

2.2.4 Feeding lines

Quantity	Unit	Nominal Thrust		Halved Thrust		Doubled Thrust	
		FU	OX	FU	OX	FU	OX
v	$[\frac{m}{s}]$	9	9	9	9	9	9
D	$[m]$	0.0017	0.0032	0.0012	0.0023	0.0024	0.0045
μ	$[Pas]$	9e-4	9e-4	9e-4	9e-4	9e-4	9e-4
Re	$[-]$	1416.5	2504.8	10016	17712	10033	35424
ϵ	$[m]$	0.0014	7.856e-4	0.002	0.011	0.001	5.55e-4
L	$[m]$	0.1694	0.2057	0.1087	0.1329	0.2629	0.3173
$Darcy$	$[]$	0.0307	0.0263	0.0338	0.0288	0.028	0.0241
ΔP_{inj}	$[Pa]$	300000	300000	300000	300000	300000	300000
ΔP_{dyn}	$[Pa]$	33210	58725	33210	58725	33210	58725
ΔP_{pipe}	$[Pa]$	100000	100000	100000	100000	100000	100000
ΔP_{valve}	$[Pa]$	20684	20684	20684	20684	20684	20684

Table 2.6: Feeding Lines Values

The length of these pipes is similar to the length of toxic one. So it doesn't affect much the trade off analysis.

2.2.5 Tank sizing

Quantity	Unit	Nominal Thrust			Halved Thrust			Doubled Thrust		
		FU	OX	PRESS	FU	OX	PRESS	FU	OX	PRESS
$P_{i,tank}$	$[Pa]$	1.6e+6	1.629e6	1.616e+7	1.6e+6	1.629e+6	1.616e+7	1.603e+6	1.629e+6	1.6161e+7
r_{tank}	$[m]$	0.239	0.3591	0.2723	0.239	0.3591	0.2723	0.239	0.3591	0.2723
t_{tank}	$[m]$	9.2814e-4	0.0014	0.008	9.281e-4	0.0014	0.008	9.2815e-4	0.0014	0.008
A_{tank}	$[m^2]$	0.7178	1.6208	0.9318	0.7178	1.6208	0.9318	0.7178	1.62	0.9318
V_{tank}	$[m^3]$	0.0572	0.194	0.846	0.0572	0.194	0.0846	0.0572	0.194	0.0846
m	$[kg]$	42.62	255.75	2.2088	42.62	255.75	2.2088	42.625	255.75	2.2088
m_{tank}	$[kg]$	1.8653	6.43	21.55	1.8653	6.43	21.5524	1.8654	6.4301	21.5524

Table 2.7: Tanks Values

2.2.6 Cooling system

It is now possible to compute the outer temperature of the wall via nodal approach.

Again, attention was payed to the cooling of the combustion chamber as it's the component where both T_{stat} and T_{tot} are the same and the highest.

Since the oxidizer mass flow rate is significantly higher than the fuel's, it is enough to rely only on it to cool the propulsion unit to avoid unnecessary complexity of the engine.

It is important to point out that, since the wall temperature in the cc is higher than the toxic propellant's case and the specific heat of the implied propellant for cooling is lower, a more performing coating was used to undergo the thermal analysis in order to reduce the heat flux and therefore to grant the system's survivability.

On a theoretical level the same coating could be used for the toxic propellant engine.

As the material compatibility of the coating was not a goal of this research further, more detailed studies should be made.

Quantity	Unit	Nominal Thrust			Halved Thrust			Doubled Thrust		
		C.C.	*Throat*	*Exit*	*C.C.*	*Throat*	*Exit*	*C.C.*	*Throat*	*Exit*
M	[-]	0.1	1	5.20	0.1	1	5.20	0.1	1	5.20
P	$[Pa]$	9.94e5	5.65e5	306.21	9.95e5	5.65e5	306.21	9.95e5	5.65e5	306.21
T	$[K]$	2.85e3	2.61e3	829.59	2.85e3	2.61e3	829.59	2.85e3	2.61e3	829.59
a	$[\frac{m}{s}]$	1.14e3	1.09e3	615	1.14e3	1.09e3	615	1.14e3	1.09e3	615
v	$[\frac{m}{s}]$	114.10	1.09e3	3.20e3	114.10	1.09e3	3.20e3	114.10	1.09e3	3.20e3
γ	[-]	1.1840	1.1858	1.2666	1.1840	1.1858	1.2666	1.1840	1.1858	1.2666
c_{pgas}	[-]	2.49e3	2.47e3	1.84e3	2.49e3	2.47e3	1.84e3	2.49e3	2.47e3	1.84e3
μ_{gas}	$[Pa*s]$	3.94e-5	9.60e-5	3.67e-6	3.94e-5	9.60e-5	3.67e-6	3.94e-5	9.60e-5	3.67e-6
λ_{gas}	$[\frac{W}{mK}]$	0.3410	0.2244	0.0892	0.3410	0.2244	0.0892	0.3410	0.2244	0.0892
ρ	$[\frac{kg}{m^3}]$	0.9010	0.5587	9.54e-4	0.9010	0.5587	9.54e-4	0.9010	0.5587	9.54e-4
A	$[m^2]$	0.0012	1.97e-4	0.0395	5.92e-4	9.86e-5	1.97e-2	0.0024	3.95e-4	0.0790
D	$[m]$	0.0388	0.0159	0.2242	0.0275	0.0112	0.1585	0.0549	0.0224	0.3171
Re	[-]	1.014e5	1.007e5	1.86e5	7.17e4	7.12e4	1.31e5	1.44e5	1.42e5	2.63e5
Pr	[-]	0.2875	1.057	0.0757	0.2875	1.057	0.0757	0.2875	1.057	0.0757
Nu	[-]	189.92	321.91	163.76	143.93	243.90	124.07	250.60	424.65	216.02
h_g	$[\frac{W}{m^2K}]$	1.67e3	4.56e3	65.18	1.79e3	4.88e3	69.84	1.56e3	4.25e3	60.80
q	$[\frac{W}{m^2}]$	1.2414e6	6.1629e6	5.3718e4	1.33e6	3.67e6	7.22e4	1.16e6	3.20e6	6.29e4
T_{aw}	$[K]$	2.84e3	2.85e3	2.32e3	2.84e3	2.85e3	2.32e3	2.84e3	2.85e3	2.32e3
σ_{Bartz}	[-]	1.2137	1.2279	1.0971	1.2137	1.2279	1.097	1.2137	1.2279	1.0971
Q	$[W]$	3.39e4	4.18e3	9.11e3	2.68e4	1.24e3	6.13e3	4.24e4	4.34e3	2.13e4
ΔT_{ox}	$[K]$	111.76	7.65	37.58	175.92	8.19	40.28	69.71	7.14	35.07

Table 2.8: Cooling Values

The result are summarize in the table below.Here there are the intial and the final temperature of the oxidizer, that must be below its $T_{boiling}$,which is 423K.

Quantity	Units	Nominal Thrust	Halved Thrust	Doubled Thrust
$T_{initial,ox}$	$[K]$	260	260	260
$T_{final,ox}$	$[K]$	417	484	371

Table 2.9: Temperature after cooling

Talking about the non nominal cases, it is quite evident that the cooling of the smaller engine is not possible with regenerative cooling and coating at the same time, since the boiling temperature of the hydrogen peroxide is around 420 K. For this case another strategy should be applied, for example the film cooling. These considerations do not apply to the double thrust sized engine, in which the mass flow rate of the available propellant for cooling is much higher.

Chapter 3

Materials and Manufacturing Process

3.1 Material compatibility

An important consideration in the design of spacecraft is the compatibility of storage materials with the propellants. Serious problems can arise because many propellants are either extremely reactive or subject to catalytic decomposition, making the selection of proper materials of construction for propellant containment and control a critical requirement for the long-life applications. The most common materials that are compatible with Hydrazine and Nitrogen Tetroxide are the Aluminum-alloys 1100, 5052, 6061, 6066, 6061-T6, 2014-T6, the Steel 304L and A286, the Titanium Ti-6Al-4V within the alloys and Tantalum and Chromium plating within the miscellaneous metals. Nitrogen Tetroxide has also a good compatibility level with Beryllium, Niobium and Tungsten. (6; 7)

It's important to take into account that Titanium reacts with nitrogen at high temperature (800°C) to form Titanium Nitride, which causes embrittlement. The compatibility with Nitrogen Tetroxide also depends highly on the moisture: water contamination causes formation of Nitric Acid, which is corrosive. It is compatible for 600 hr at 135°C, there is no significant corrosion during exposure of specimens to N_2O_4 containing up to 0.2% wt water within the temperature range of -9 to 74°C and it is virtually unattacked by N_2O_4 containing up to 3.2% wt water at temperatures up to 74°C.

More recent studies have led to the utilization of new, more complex and more performing alloys such as Inconel718 and Inconel625, which are Nickel-based superalloys widely used in hot conditions, and also as JBK-75 and NASA-HR-1, which are high-strength Fe-Ni-based superalloys. (16) While Inconel is reportedly compatible with Hydrazine, there aren't clear data about its compatibility with Nitrogen Tetroxide: further analysis would be necessary. A quite new solution that could be interesting is also GRCop, originally developed at GRC. It is a high conductivity, high-strength, dispersion strengthened copper-alloy for use in high-temperature and high heat flux applications. NASA has completed significant material characterization and testing, along with hot-fire testing, to demonstrate that GRCop-42 and GRCop-84 alloys are suitable for use in combustion chambers. Additional development and testing has been completed on AM bimetallic chambers using GRCop-84 liners and superalloy jackets, fabricated using two Directed Energy Deposition (DED) processes: Electron Beam Freeform Fabrication (EBF³) and Blown Powder DED. However, NASA has tested these combustion chambers only with LOX/Hydrogen, LOX/Methane, and LOX/Kerosene propellants making necessary a test campaign to assure the compatibility with the propellants of this mission. (14; 15)

For the green propellants the literature about materials compatibility is quite restricted. Since Kerosene is widely used, the more concerning is the behavior of HTP. A limited set of common materials can be used with this propellant, such as pure aluminum 1060, fully austenitic stainless steel with passivation and conditioning, Teflon and polyethylene. An ESA

activity with European Astrotech Ltd in the UK has investigated the compatibility between a variety of current and future materials and weld combinations. In this activity HTP was shown to be incompatible with Titanium or SS347, while Al2060 EB, SS316 and SS304 may be compatible with HTP if given longer pre-exposure prior to loading.

3.2 Additive Manufacturing

For specif info on PBF, SLM and DLD see appendix B.

The use of PBF technology for fabrication of liquid propellant rockets components is known, a CVP (Counter Rotating Vortex) has been built by Park using this method on Inconel 718 powder (20).

This technique is also effective for fabrication of rocket components with embedded cooling system, since such complex geometry benefit from additive manufacturing. Catina et al. demonstrated PBF printed Inconel 625 highly-customized injector plates with double swirl structure (21).

In addition to these research studies, Airbus Safran Launchers reported injectors manufactured with PBF using Inconel 718 and 316L for liquid rocket engines with substantial reduction in production cost and manufacturing time (22).

PBF printed rocket components shows clear and numerous advantages compared to other processes, starting with reduction in cost and parts. As for every Additive manufactured method and product, production of each combustion chamber will require long time, especially since the precision required for the injection orifices is high.

In PBF options there's the SLM method: literatures have shown that SLM is capable of fully melting the powder material, producing fully dense near net-shape components without the need for post-processing, other than the removal of parts and supports from substrate plate. This makes SLM a superior Additive Manufacturing (AM) process compared to SLS, which binds powder materials via solid state sintering or melting of binding agents, resulting in parts with high porosity and low strength (23).

After steel and titanium materials, nickel-based alloy is the most studied group of metals for the SLM process. Most of these publications are on Inconel, a family of nickel-based superalloys typically used in high-temperature applications. Nickel-based alloys studied for the SLM process include Inconel 625, Inconel 718, Chromel, Hastelloy X, Nimonic 263, IN738LC, and MAR-M 247. Many of these publications focus on the process parameters for formation of stable melt track since it is a pre-requisite of forming fully dense 3D components.

Another possibility of PBF is the DLD, that is collecting interest in aerospace industries due to the cost saving that the process can offer. Powder characteristics have a great impact on the quality and properties of the DLD manufactured parts. Chemical composition of powders, particle size, distribution and morphology together with laser parameters, laser power, power feed rate and scanning speed, have to be optimised in order to produce parts with required physical and mechanical properties (24). Another important DLD processing parameter is the hatching or scanning strategy that defines the path of the powder deposition head. The microstructure and mechanical properties of the DLD parts can be controlled by varying the hatching strategy (25). Additionally, the nozzle inclination angle and the set focal plane for the laser beam are important factors affecting the properties of the DLD parts (26).

The DLD is commonly used to process the following materials: nickel-based alloy (In625, In718, In738, In713, In939, CM-247LC, Nimonic 263, Hastelloy X, Hastelloy C-276, Waspaloy, Haynes 230, MarM247), titanium alloys (Ti6Al4V, Ti-6-2-4-2, Ti-6-2-4-6, CP Ti), aluminium and its alloys (4047, 6061, 7050, 7075, AlSi7Mg, AlSi10Mg, AlSi12), ron-based alloys (17-4PH, H13, 304L, 316L, 420SS, PH 138 Mo, 155PH, AISI 4140), cobalt-based alloys (Stellite21, CM-64, Co6, CoCr) and copper-based (Cu-Ni) and iron-nickel-chromium alloy (A286) (27).

Material Deposition Method	Printable Materials	Layer Resolution	Advantages	Disadvantages
Laser fusion of powder	Metals, Thermo-plastics	20-100 μm	High resolution	Expensive, post-curing needed, low yield of production, low mechanical properties

Table 3.1: Characteristics of PBF used on rocket components

3.3 Material selection for injection plate and engine case

Material	Density [kg/m^3]	Yield strength [Mpa]	Thermal Conductivity [W/mK]
A286	7920	275	15,1
Zirconia	5680	230	2,2
Al2219	2800	76	170
Ti6Al4V	4430	880	7.1

Figure 3.1: Properties of the suggested materials

The material indicated for the injection plate is the austenitic stainless steel A286. It is an iron-base superalloy useful for applications requiring high strength and corrosion resistance. It is chemically compatible with both of the couples of propellant considered. It is also suitable for additive manufacturing processes. The sizing of holes imposes as a constraint a diameter of 0,977 mm for the fuel and a diameter of 0,83 mm for the oxidant. A laser fusion of powder is indicated for the realization of these holes, and A286 is compatible with it, as stated in the previous paragraph. In particular it is indicated the DLD possibility.

For the fuel tank the choice falls on the Al2219 alloy that belongs to the aluminium-copper family. The choice of these material is motivated by it's own compatibility with the fuels at the liquid state and the lower density that brings a mass save for the tanks.

The A286 has it's also suggested for the helium tank. The ultimate tensile strength is very high and suitable to hold up the high pressure of helium, while keeping a low tank thickness.

The A286 finds the last spot in the material of the combustion chamber and in the convergent trait of the nozzle. This is mandatory since the injection plate and the combustion are made in a single block. Also it is compatible with the material suggested for the thermal coating: zirconia, or zirconium dioxide (19). This is a ceramic material with a very low thermal conductivity. Researches suggest that it is even feasible with additive manufacturing (18). It can be argued that A286 has a low thermal conductivity, and a coating is not needed. However the A286 melting point is between 1370 K and 1430 K, making it necessary to find a solution because of the temperature reached in the combustion chamber. The solution is exactly the zirconia, with a 2,988 K melting point.

The divergent trait of the nozzle is indicated to be made in a titanium alloy: the Ti6Al4V. It has half of the density of steels, so that there's a considerate save in weight. Researches suggest that it is feasible cold spray additive manufacturing (17), however the studies are still on going. Most importantly it doesn't melt at the temperatures reached in nozzle expansion, since it has a 1298,7 K melting point.

Chapter 4

Results

4.1 Final comment and propellant trade-offs

The work that has been done shows that the green, low-toxic propellant can grant a higher specific impulse and therefore is worth considering for the examined application. The choice of the green propellants' couple would also assure a mass saving: less propellant is needed to obtain the same thrust level; this could be traduced in a higher payload mass. Once these considerations were done, it seems to be more convenient to choose it as the propellant couple of the engine, so the kerosene and hydrogen engine is worth exploring. On the other end, the lower density of RP-1 and Hydrogen Peroxide, in comparison with Hydrazine and Nitrogen Tetroxide, would lead to a slight increase of the total volume of the tanks: it's therefore necessary to verify that this would not constitute a problem for other aspect of the mission, such as the launch phase.

It shall also be considered that, to achieve the system's survivability, an efficient cooling system, one that grants the hydrogen peroxide to stay in its safe operative temperature range, is designed because this oxidizer has a higher freezing point, similar to water's.

The chosen green propellant for this engine is compatible with the materials chosen for the toxic engine, making it a viable option to consider since it does not require additional studies regarding material compatibility. Therefor the same AM techniques can be used when entering the manufacturing phase.

It is also important to notice that, since at the moment the 98%HPT/RP-1 couple has never been used or tested, a more precise study should be done to determine its behaviour: this would lead to additional costs.

Scaling up the engine is convenient under the hypothesis used all throughout the design phase because larger engines are easier to cool down. The most critical point of this green propellant is the challenging procedure of scaling down the engine because the main coolant propellant of this green couple has a smaller specific heat capacity with respect to the hydrazine. The overall consideration make still the above-mentioned engine a suitable option for a low thrust, high impulse kick-stage.

Appendix A

Workflow

A.1 Nozzle sizing

To size the nozzle both a conical and a bell nozzle configuration are considered. The sizing is made with the throat area value computed into the general performance analysis section and the expansion ratio is fixed. The throat area is computed:

$$A_t = \frac{T_{1D}}{P_c c_f} \tag{A.1}$$

Thus the exit area is computed as the product between the expansion ratio and the throat area. As there are not specific constrains on the nozzle manufacturing, the angles of both the convergent and divergent part are chosen freely and according to typical values for such angles: $\alpha = 15°$, $\beta = 40°$. A key parameter needed to perform such calculations is the combustion chamber contraction ratio. As a general rule the ratio should be less than 6. A very good number for efficiency is around three. Since this would imply for the combustion chamber of the toxic couple a very high length it has been decided that the contraction ratio should be at least 4. By imposing this value a reasonable Mach number in the combustion chamber is achieved after inverting the following formula:

$$A_c = \frac{A_t}{M_c} \left[\frac{2}{\gamma + 1} \left(1 + \frac{\gamma - 1}{2} M_c^2 \right) \right]^{\frac{\gamma+1}{2(\gamma-1)}} \tag{A.2}$$

The length of both the convergent and divergent section is computed as:

$$L_{conv} = \frac{r_c - r_t}{tan(\beta)} \tag{A.3}$$

$$L_{div} = \frac{r_e - r_t}{tan(\alpha\ )} \tag{A.4}$$

A parameter to take into account losses due to the 2D nature of the flow should be used to regulate the real thrust value.

$$T_{2D} = \lambda T_{1D} \tag{A.5}$$

$$\lambda = \frac{1 + cos(\alpha)}{2} \tag{A.6}$$

The bell nozzle design using RAO model, is implemented with real life usability in mind for this engine, hence, although no constrains are given on the length nor the weight of the engine we opted for a 60% length and a 97% efficiency as inputs to minimize the weight, accepting

a minor performance drawback in terms of stability. To size the RAO model, the graphs for the relations between efficiency, length ratio and the exit area ratio are interpolated beneath a MATLAB code to obtain the final result. By imposing two out of these three parameters it is possible to obtain the third one and the angles at the beginning and at the end of the parabolic shaped like region of the nozzle.

The RAO model gives also a rule of thumb of how the throat region should be modelled by imposing two circular curves for convergent and divergent parts, whose radii are respectively 1.5 and 0.382 times the radius of the throat. The reference (29) explains how the three coefficients of the parabolic function should be obtained and the final step consists in solving a 2 equations system, where the variables are the coordinates of intersection point between circular and parabolic section, by imposing the continuity of the two functions and their derivatives.

A.2   Combustion chamber sizing

For the sizing of the combustion chamber, a very important parameter is the characteristic length L*, defined as well:

$$L^* = \frac{V_c}{A_t} = \frac{\dot{m}_p}{\rho A_t} t_{res} \tag{A.7}$$

where V_c is the combustion chamber volume and t_{res} is the residence time in the combustion chamber. This is not representative of a physical length and is strictly linked to the couple of reactants. The value is typically derived from the experience of similar engine already built (9).

Once that L^* is known, from the Eq.(A.7), is possible to retrieve the combustion chamber volume, and knowing the section of the combustion chamber Eq. (A.2) , is possible to compute the chamber length L_c :

$$L_c = \frac{V_c}{A_c} \tag{A.8}$$

A.3   Injection plate sizing

The minimum diameter of the injection orifices is chosen as a starting point for the design. Hence, the considered additive manufacturing can only achieve diameters higher than 0.5 mm. This way, at the end of the injection plate's design, the minimum value between the two will be certainly higher than this threshold, as it will be shown. Thus, the minimum area can be computed and, once the pressure drop has been assumed, the mass flow rate of one single injector can be obtained:

$$\dot{m} = AC_d\sqrt{2\Delta P \rho} \tag{A.9}$$

By doing the ratio between each total propellant mass flow rate and its respective value from above it is possible to compute for both propellants the number of needed injectors, N_f and N_{ox}. Both groups of injectors will be divided in pairs for the final positioning on the plate, since the couple configuration is chosen; in this way, by halving and rounding by excess the minimum value between the two, the integer number of orifice couples for the respective propellant is obtained. Finally, after computing the ratio between the total numbers of orifices for fuel and oxidizer and after rounding this value, the integer number of the orifices for the remaining propellant is also fixed.

Knowing the value of mass flow rate and real section area for the injectors the exit velocity can be easily computed using the continuity equation of the mass. At the end the check of this

last value must be done. Typical numbers of exit velocity for a good atomization to propellant droplets in the combustion chamber are around 20-30 m/s. To achieve such a value the only possible ways are either to increase the pressure drop along the injectors or to increase the discharge coefficient of the injectors. For the pressure drop a value of 0.35 times the chamber pressure is chosen. This is quite a high number to be chosen for a non throttleable rocket engine, whose value can be approximated as a rule of thumb around 0.2 the chamber pressure, and it is implying higher pressures upstream, thus increased mass for the feeding lines and tanks. On the other hand, having a higher number brings a beneficial effect by isolating more the feeding system from the the combustion chamber, which can be quite important for a hypergolic liquid combustion chamber.
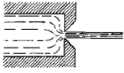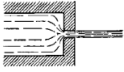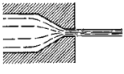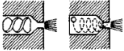
A.5   Orifice types

Orifice Type	Diagram	Diameter (mm)	Discharge Coefficient
Sharp-edged orifice		Above 2.5 Below 2.5	0.61 0.65 approx.
Short-tube with rounded entrance $L/D > 3.0$		1.00 1.57 1.00 (with $L/D \sim 1.0$)	0.88 0.90 0.70
Short tube with conical entrance		0.50 1.00 1.57 2.54 3.18	0.7 0.82 0.76 0.84–0.80 0.84–0.78
Short tube with spiral effect		1.0–6.4	0.2–0.55
Sharp-edged cone		1.00 1.57	0.70–0.69 0.72

Figure A.1: Injection Holes

The selection of the hole design for the injectors is based on the selected diameter by using some tabulated references and can be exploited to further increase the velocity of the exiting jet, hence a higher diameter can imply an increase of the discharge coefficient.

As already mentioned the coupled like-on-like configuration is used. Since both streams have the same velocity and mass flow rate there is no need for finding the transversal balance equilibrium when an axial resultant flow is desired. However it is known for a hypergolic propellant combustion chamber with a like-on-like impingement that a flow directed towards the center with an angle between 2 and 5 degrees can be beneficial for a better mixing and faster combustion, thus improving the combustion chamber performance. A consideration should be done also on the distance of the convergence point of the two streams from the injection plate to prevent its melting due to excessive heat transfer. From the literature (11) it is suggested to adopt a distance of the impingement from the plate not grater than 5 times the diameter of the orifices and for greater performance a fan cant angle of around 41 degrees, as it is shown in the figure A.2a

The distance between the injectors is also computed and the momentum balance is applied to impose a flow directed with 3 degrees with respect to the axial direction. The final velocity of the propellant is also required so another equation is required to have a fully determined system and to do so the trigonometric relation between the orifices' distance and the two angles can be exploited. The unknown variables of the problem are then three: the two γ angles of the jets with respect to the axial direction and the final velocity v_p after the impingement as it

is shown in the formulas:

$$\dot{m}_p v_p sin(\beta) = \dot{m}_{ox} v_{ox} sin(\gamma_{ox}) - \dot{m}_f v_f sin(\gamma_f) \tag{A.10}$$

$$\dot{m}_p v_p cos(\beta) = \dot{m}_{ox} v_{ox} cos(\gamma_{ox}) + \dot{m}_f v_f cos(\gamma_f) \tag{A.11}$$

$$D_{orifices} = D_{plate}(tan(\gamma_f) + tan(\gamma_{ox})) \tag{A.12}$$

where $D_{orifices}$ and D_{plate} are respectively the distance between the two injectors and the distance of the impingement from the plate.

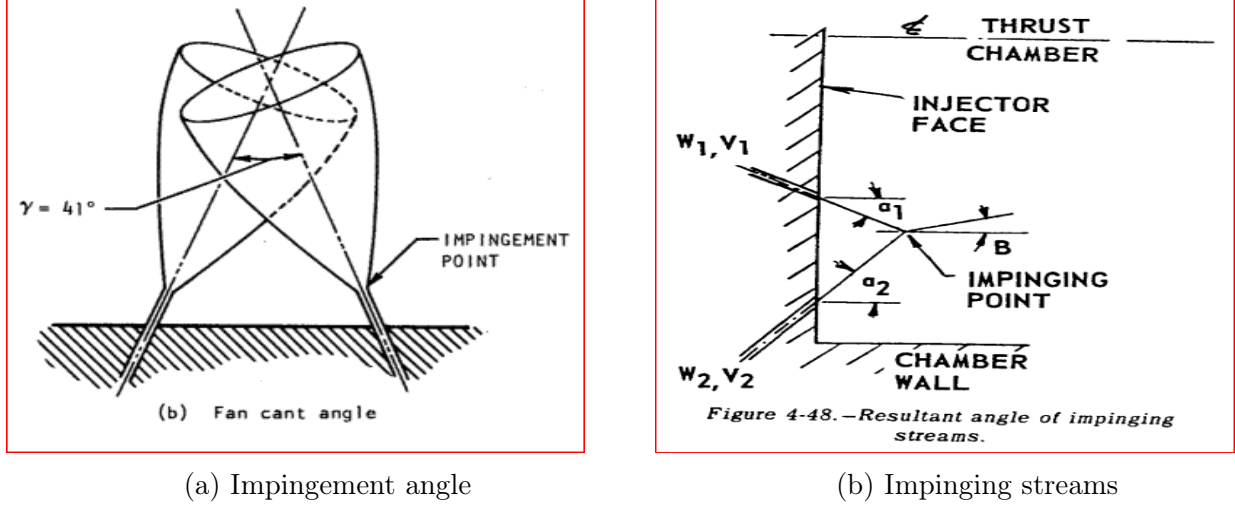(a) Impingement angle

(b) Impinging streams

Figure A.2: Impinging and resultant angles for a couple of injectors

A.4 Feeding lines sizing

The propellant feed system include all the elements between the tanks and the combustion chamber, so in the analysis are includes the propellants feed lines, valves and all the elements needed for safe and reliable operation. The goal in the design of the feed lines is to minimize the pressure drops δP_{feed} as much as possible. From the literature (10) is know that the limit is in a range between 35000 Pa and 50000 Pa.So in order to keep these values of pressure drops, we assume the propellant flow rates (v) around 10 m/s.

By applying the continuity equation, is possible to compute the pipe's area and so the diameter of each feed lines:

$$A_c = \frac{\dot{m}}{\rho v} \tag{A.13}$$

Finally, the length of the pipe is computed by reverse the equation:

$$\Delta P_{feed} = \frac{8}{\pi^2} f \frac{\dot{m}^2}{\rho} \frac{L}{D^5} \tag{A.14}$$

A.4.1 Valves

As High level requirements, the engine should have no throttling capability, but just on/off. So the selection of an on/off valve is done. This category include simple valve (ball,needle,gate), that can only start and stop the flow, without throttling capability. Due to the very low dimension of the entire system, the choice of the valves fell on the ones with a diameter compatible with pipe's diameter and that respect the physical's constraints like pressure. Some possible options can be found in the catalogue of Vacco (30) , where are report a lot of valves for space application.

A.5   Tank sizing

A.5.1   Propellant Tanks

As requirement for the design of the engine, there is the realization of a Standard pressure-fed regulated architecture with separate tanks and feeding lines. The pressure needed in the tanks in order to guarantee the right mass flow rate, must be equal to the sum of chamber pressure and all the drops through the feed system:

$$\Delta P_{tank} = P_c + \Delta P_{dyn} + \Delta P_{valve} + \Delta P_{feed} + \Delta P_{cool} + \Delta P_{inj} \tag{A.15}$$

where ΔP_{dyn} are the dynamic losses computed by knowing the velocity of the flows in the feeding lines:

$$\Delta P_{dyn} = \frac{1}{2}\rho V^2 \tag{A.16}$$

The volume of the tanks is given by the sum of four contributes:

$$V_{tot} = V_{pu} + V_{ull} + V_{trap} \tag{A.17}$$

where:
V_{tot} is the total tank volume
V_{pu} is the usable propellant volume, retrieved form the propellant mass
V_{ull} is the ullage volume, the volume of tank left unfilled to allow expansion or contraction of the tank structure
V_{trap} is the volume of the unusable propellant left in the feed lines, valves, tank and other component. Is assume equal to the feed line volume.
An useful check can be done with the follow equation:

$$P_{tank} = \left[10^{-0.1281[log(V_{tank})+0.2498]}\right] \times 10^6 \tag{A.18}$$

or using the chart from the Nasa SP-8112 (12). For the shape of the tanks, is select a spherical shape, more complex due to positioning problems, but with higher performances, since they can offer the most volume for a given surface area. For a preliminary design of the tanks, are consider only pressure loads since it is the greatest effect on the tank structural requirements.So from the Volume formula is compute the radius of the tank:

$$r_t = \frac{3}{4}\left(\frac{V_t}{\pi}\right)^{1/3} \tag{A.19}$$

and next the thickness of the tank:

$$t_t = \frac{r_t p_b}{2\sigma_y} \tag{A.20}$$

where:
σ_y is allowable material strenght Pa
p_b is the burst pressure, computed as the product between a safety factor f_s (choose as 2) and the Maximum Operating pressure of the tanks, that is the initial pressure of the tank, since it is constant.
After computing the surface area of the tanks ($A_t = 4\pi r_t^2$), and the selection of the compatible material for the tanks (ρ_t), is possible to retrieve the mass of the tanks as:

$$m_t = \rho_t A_t t_t \tag{A.21}$$

A.5.2 Pressurant Tank

The stored gas choose for pressurize the propellants tank is the Helium, since it is inert and lightweight (low molecular mass), but it is bit more expensive.

γ	M_{mol}	T_i
1.67	4 g/mol	298 K

Table A.1: Properties of Helium

The mean value between the two pressures in the oxidizer and fuel tanks is select as p_f for the pressurizer, while as p_{in} a pressure ten times the initial one is imposed. Considering an isentropic flow, thus no change in temperature, it is possible to compute the final temperature of the pressurizer gas:

$$T_f = T_i \left(\frac{p_f}{p_i} \right)^{\frac{\gamma-1}{\gamma}} \tag{A.22}$$

As suggested from the literature (10) it has been decided to implement an iterative method for the computation of the volume and mass of the pressurizer. The following steps are being undertaken inside the *while* cycle, after initializing the volume of the pressurizer tank:
- The total volume of the gas at the final condition is given by the sum of the three tanks.
- The mass of the pressurizer is obtained using the ideal gas equation.
- The new iterated volume of Helium is computed using still the the same equation but at the initial condition.
- When the absolute value of the difference between the last two iteration is relatively law it is possible to stop the cycle.
So after the iterative cycle is retrieve the volume of the tank of the gas from:

$$m_{press} = \frac{V_{t,press} p_f}{R T_f} \tag{A.23}$$

Finally the mass of the tank is computed as before:

$$m_{ptank} = \rho_p V_{ptank} \tag{A.24}$$

Where V_{ptank} represents the volume physically occupied by the mass of the tank, computed as the difference between the external and internal volume, assuming the thickness is already computed using the A.20 equation.

A.6   Cooling system

In order to perform a preliminary choice of the cooling system a thermal analysis was required. We were interested into mapping the heat flux in the combustion chamber, nozzle throat and exit. For this the CEA software offered by NASA is required to obtain thermal transport properties such as viscosity, specific heat capacity and conductivity. All the properties necessary to compute the heat flux in correspondence of the three sections are thus calculated. For the computation of the total heat flow along the engine area the assumption of constant properties of plate and throat section along respectively the cylindrical and convergent part of the engine is called. For more precise estimation along the divergent nozzle the CEA software is used to

obtain the thermal transport properties in correspondence of 5 different sections of the nozzle to be able to compute the thermal flux also in the central part of the divergent. Doing the same procedure for the convergent part would be unnecessary for a preliminary phase design, since the it has a very restricted length.

Different simulations changing each time either the material used for the nozzle, the correlations used to obtain the convective heat transfer coefficient or the cooling strategy are undertaken. As a benchmark for the convective heat transfer coefficient a first simulation is ran using the Dittus Boelter correlation to define the Nusselt number, thus the convective coefficient:

$$Nu_D = 0.0265 Re_D^{0.8} Pr_D^{0.3} \tag{A.25}$$

which implies a Prandtl number higher than 0.7 to be considered a good approximation of reality. Since it was noted for this nominal design that the Prandtl number is not satisfying the initial assumption the Cinjarew correlation for the combustion chamber and the Bartz correlation for the throat and nozzle exit are used. The Cinjarew Correlation is

$$Nu_D = 0.0162(Re_D Pr_D)^{0.82}(\frac{T_{stag}}{T_{wall}})^{0.35} \tag{A.26}$$

whereas T_{stag} is defined as

$$T_{stag} = T_{stat} + C_R(T_0 \eta_{nozzle}^2 - T_{stat}) \tag{A.27}$$

The Bartz Correlation is

$$Nu_r = 0.026 Re^{0.8} Pr^{0.4}(\frac{d_{th}}{r_{cc}})^{0.1}\sigma_B \tag{A.28}$$

Where σ_B is defined as follows

$$\sigma_B = \left[0.5\frac{T_{wall}}{T_{stag}}(1 + \frac{\gamma - 1}{2}M_a^2 + 0.5)\right]^{-0.68}\left[1 + \frac{\gamma - 1}{2}M_a^2\right]^{-0.12} \tag{A.29}$$

It is important to notice that the characteristic length used in the Bartz correlation is NOT the diameter of the channel but it's its radius.

After the Nusselt Number is computed the convective heat transfer coefficient is obtained

$$h = \frac{kNu}{d} \tag{A.30}$$

We established that these correlations tend to give a lower convective heat transfer coefficient than the DB. The nodal approach is used to perform the thermal analysis.

The major constrain imposed is the inner wall temperature of the nozzle as it depends on the material: we considered both Incoloy alloy A286 and Inconel alloy 718.

The heat flux among the hot gas mixture and the inner wall of the nozzle is computed through Newton's Law.

$$q = h(T_a - T_w) \tag{A.31}$$

As an engineering choice is required, the thickness of the nozzle wall is fixed so that, knowing the temperature on the outer side, it is possible to impose an equilibrium condition among the heat flux coming from the hot gas mixture and the conductive one through the wall of the nozzle

$$\Delta T = \frac{t_h q}{k} \tag{A.32}$$

$$T_{out} = T_w - \Delta T \tag{A.33}$$

It could be verified that a radiative-only cooling system is not feasible as the radiative power emitted by the nozzle at the before mentioned outer temperature is too low to grant the continuity of the heat flux (under the assumption of a emissivity of 0.9 and a view factor of 1)

$$q_{rad} = \epsilon \sigma_0 T_{out}^4 \tag{A.34}$$

this increases the nozzle temperature to unwanted values. A solution including regenerative cooling is then considered. For this only a global design is undertaken to see if the total heat capacity of the propellant is enough to satisfy the cooling of the whole nozzle below a certain maximum operating temperature. The local problem will not be considered. The convective heat transfer coefficients of the hot gas mixture inside the nozzle were computed using the Bartz correlation.

It could be noticed right away that the heat capacity of the fuel is too low, thus the temperature reached in the cooling channels would be too high and the fuel itself would not be able to withstand it without decomposing. In order to increase the operating temperature of the system and reduce the heat flux through the components a coating layer is added on the inside wall of the combustion chamber and the convergence part of the nozzle, up to the throat.

This material, namely zirconium oxide, with higher thermal properties than the metal, allowed to have a wall temperature of 1500 K inside the chamber. However, the titanium alloy-made nozzle is capable of standing temperatures of 1000 K without any insulation layer, so that temperature has been considered as wall temperature for the thermal analysis. This solution enables the system to operate in nominal conditions without affecting the properties of the fuel. This analysis is also performed using a nodal approach. As only a thermal analysis is required, a check on the mechanical compatibility of the coefficient of thermal expansion among the coating layer and the nozzle was not performed and a perfect adhesion between the materials and no heat flux dispersion are assumed. A more refined analysis will have to be performed at a latter moment.

Appendix B

Additive Manufacturing

As a novel and highly innovative AM technique, PBF relies on a laser to fuse together powder rapidly, sometimes under inert gas atmosphere, especially to provide a protective measure against oxidation. As opposed to filament or resin, the material is used in powder form as a stock on which a roller slides and deposits a prescribed amount of powder onto a build plate in a layer-by-layer fashion. In this method, ideally, the powder is required to have spherical geometry with monomodal distribution to ensure high flowability and small surface area to volume ratio for high packing of the prints. Selective Laser Melting (SLM) is an additive manufacturing process developed by Dr. M. Fockele and Dr. D. Schwarze of F & S Stereolithographietechnik GmbH, with Dr. W. Meiners, Dr. K. Wissenbach, and Dr. G. Andres of Fraunhofer ILT to produce metal components from metallic powders. It is a powder bed fusion process that uses high intensity laser as an energy source to melt and fuse selective regions of powder, layer by layer, according to computer aided design (CAD) data. The patent for this technology was first applied in 1997 to the German Patent and Trade Mark Office and published in 1998 (28).

The DLD (Direct Laser Deposition) technology employs a focused laser beam to fuse materials in the form of metal wires and/or powder onto a building platform and thus producing parts layer by layer [reference]. During the DLD process, some of the laser irradiation is absorbed by the substrate on which the powder particles are delivered through a nozzle and thus a controlled melt pool is created in the laser-material interaction area [reference]. Additionally, an inert gas, for example argon, is delivered onto the deposition area in order to minimise any metal oxydation.
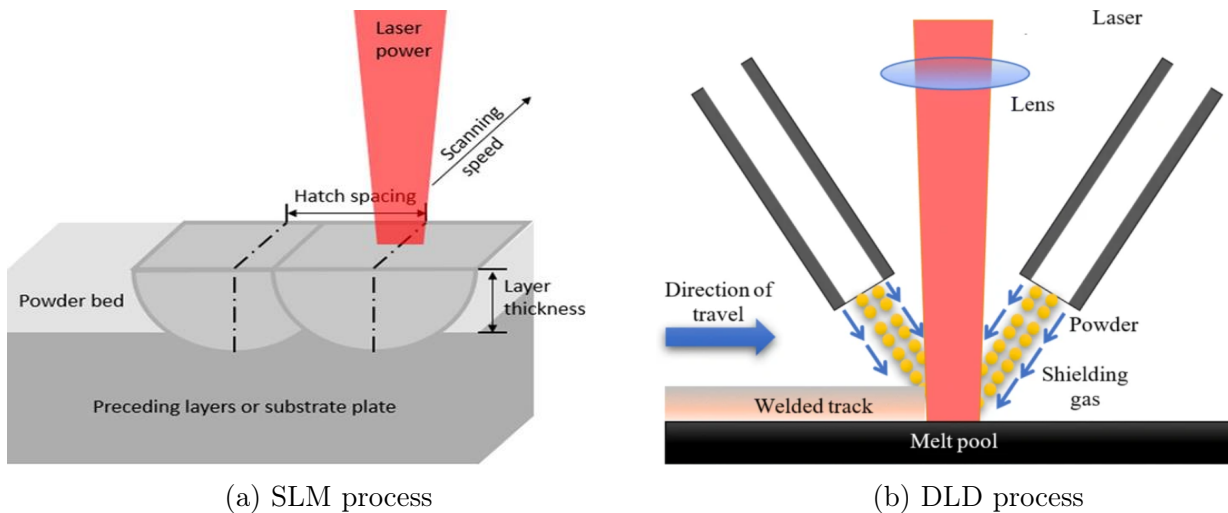

(a) SLM process

(b) DLD process

Figure B.1: Impinging and resultant angles for a couple of injectors

Bibliography

[1] R. Schmidt, J. D. Credland, A. Chicarro, Ph. Moulinier. ESA's Mars Express Mission – Europe on Its Way to Mars. *ESA*, bulletin 98, June 1999.

[2] Donald Savage, Michael Buckley. MESSENGER, NASA's Mission to Mercury. *NASA*, launch press kit, August 2004.

[3] Venkatesan Sundararajan. Mangalyaan - Overview and Technical Architecture of India's First Interplanetary Mission to Mars. *AIAA Space*, San Diego, California, September 10-12, 2013.

[4] Stefania Carlotti, Filippo Maggi. Evaluating new liquid storable bipropellants: Safety and performance assessments. *Aerospace*, 9(10):561, 2022.

[5] Lily Blondel-Canepari, Livia Ordonez Valles, Martin Tajmar et al. Roadmap Towards a Greener Kick-Stage Propulsion System. *73° International Astronautical Congress*, Paris, France, September 18-22, 2022.

[6] Robert Lechler. Literature Survey of Materials compatible with Propellants. *German Aerospace Center*, October 20, 2015.

[7] P. E. Uney, D. A. Fester. Material Compatibiilty with Space Storable Propellants, Design Guidebook. *NASA-JPL*, Pasadena, California, March 1972.

[8] G. H. Vatistas, S. Lin, C. K. Kwok. Reverse Flow Radius in Vortex Chambers. *AIAA Journal*, Vol. 24, No. 11, pp. 1872-1873, 1986.

[9] George P. Sutton, Oscar Biblarz. Rocket propulsion elements, Ninth Edition. John Wiley & Sons, 2017.

[10] Wiley J. Larson, Gary N. Henry, Roland W. Humble. Space Propulsion Analysis and Design. *McGraw-Hill*, 1995.

[11] G. S. Gill, W. H. Nurrick. Liquid Rocket Engine injectors. *NASA-SP-8089*, March 1, 1976.

[12] J. C. Lee, P. Ramirez. Pressurization Systems for Liquid Rocket. *NASA-SP-8112*, October 1975.

[13] Enes Akca, Ali Gursel. A Review on Superalloys and IN718 Nickel-Based INCONEL Superalloy. *Periodicals of Engineering and Natural Sciences*, Vol. 3, No. 1, 2015.

[14] Paul R. Gradl, Dr. Christopher S. Protz, Dr. David L. Ellis, Sandy E. Greene. Progress in Additively Manufactured Copper-Alloy GRCop-84, GRCop-42, and Bimetallic Combustion Chambers for Liquid Rocket Engines. *Washington D.C., United States*, October 21-25, 2019.

[15] Paul R. Gradl, Chris Protz, John Fikes, Allison Clark. Lightweight Thrust Chamber Assemblies using Multi-Alloy Additive Manufacturing and Composite Overwrap. *AIAA Propulsion and Energy 2020 forum*, August 2020.

[16] Po-Shou Chen, Michael Mitchell. ALLOY NASA-HR-1. *Aerospace Structural Metals Handbook*, April 2005.

[17] Congcong Cao, Wenya Li, Zhengmao Zhang, Xiawei Yang, Yaxin Xu. Cold Spray Additive Manufacturing of Ti-6Al-4V: Special Nozzle Design Using Numerical Simulation and Experimental Validation. *Coatings*, February 6, 2022.

[18] Xiuping Zhang, Xin Wu, Jing Shi. Additive Manufacturing of Zirconia Ceramics: a State-of-the-Art Review. *Journal of Materials Research and Technology*, Vol. 4, No. 9, pp. 9029-9048, July-August 2020.

[19] Y. Adraider, Y.X. Pang, F. Nabhani, S.N. Hodgson, M.C. Sharp, A. Al-Waidh. Fabrication of Zirconium Oxide Coatings on Stainless Steel by a Combined Laser/Sol–Gel Technique. *Ceramics International*, Vol. 39, No. 8, pp. 9665-9670, December 2013.

[20] Jeongmoon Park, Stephen D. Heister, John Sullivan. Development of a Counter-Rotating Vortex Pair (CVP) Mixer for Aerospace Applications. *49th AIAA/ASME/SAE/ASEE Joint Propulsion Conference*, San Jose, California, July 12, 2013.

[21] James J. Catina, Brett Nellis, Devan Grigsby, Kristen Castonguay. Use of Additive Manufacturing to Develop Advanced Hybrid Rocket Designs. *52nd AIAA/SAE/ASEE Joint Propulsion Conference*, Salt Lake City, Utah, July 22, 2016.

[22] Sebastian Soller, Alexandre Barata, Steffen Beyer, Arne Dahlhaus, Didier Guichard. Selective Laser Melting (SLM) of Inconel 718 and Stainless Steel Injectors for Liquid Rocket Engines. *Space Propulsion Conference 2016*, Rome, Italy, May 2016.

[23] C. Y. Yap, C. K. Chua, Z. L. Dong, Z. H. Liu. Review of selective laser melting: Materials and applications. *Applied Physics Reviews*, Vol. 2, No. 4, December 2015.

[24] Benjamin Bax, Rohan Rajput, Richard Kellet, Martin Reisacher. Systematic evaluation of process parameter maps for laser cladding and directed energy deposition. *Additive Manufacturing*, Vol. 21, pp. 487-494, May 2018.

[25] Katherine L. Terrassa, Thale R. Smith, Sen Jiang, Joshua D. Sugar, Julie M. Schoenung. Improving build quality in directed energy deposition by cross-hatching. *Materials Science and Engineering: A*, Vol. 765, September 23, 2019.

[26] Gangxian Zhu, Shihong Shi, Geyan Fu, Jianjun Shi, Shi Yang, Weidong Meng, Fubing Jiang. The influence of the substrate-inclined angle on the section size of laser cladding layers based on robot with the inside-beam powder feeding. *The International Journal of Advanced Manufacturing Technology*, Vol. 88, pp. 2163-2168, May 27, 2016.

[27] MSc. Jana Kelbassa, Dr. Andres Gasser, Dr. Norbert Pirch. WIRE VS. POWDER IN LMD. *LAM Conference 2018*, Schaumburg, Illinois, March 29, 2018.

[28] WilhelmMeiners, Dr. KonradWissenbach, Dr. AndresGasser. Shaped body especially prototype or replacement part production. *Granted patent, patent number DE 19649849 C1*, Germany, February 12, 1998.

[29] K. R. Sreenath, A. K. Mubarak. Design and analysis of contour bell nozzle and comparison with dual bell nozzle.*International Journal of Research and Engineering*, Vol. 03, No. 06, June 2016.

[30] https://www.vacco.com/images/uploads/pdfs/latch_valves_low_pressure.pdf